JOURNAL OF AGRICULTURAL AND FOOD CHEMISTRY

Article

pubs.acs.org/JAFC

Modeling the Interfacial Interactions between CrtS and CrtR from *Xanthophyllomyces dendrorhous*, a P450 System Involved in Astaxanthin Production

Jennifer Alcaíno,[†] Matías Fuentealba,[‡] Ricardo Cabrera,[‡] Marcelo Baeza,[†] and Víctor Cifuentes*[,†]

[†]Centro de Biotecnología y Departamento de Ciencias Ecológicas and [‡]Departamento de Biología, Facultad de Ciencias, Universidad de Chile, Las Palmeras 3425, Casilla 653, Santiago, Chile

ABSTRACT: *Xanthophyllomyces dendrorhous* is a natural source of astaxanthin, a carotenoid widely used in the food industry. In this yeast, astaxanthin is synthesized from β-carotene by a cytochrome P450, CrtS, which depends on CrtR, the four-domain cytochrome P450 reductase (CPR). Although *Saccharomyces cerevisiae* has an endogenous CPR (*Sc*CPR), expression of CrtS does not result in astaxanthin production unless it is coexpressed with CrtR. Assuming that CrtS could interact with the FMN-binding domain of either CrtR or *Sc*CPR (*Xd*FMNbd and *Sc*FMNbd, respectively), the aim of this work was to identify possible interaction differences between these alternative complexes by protein modeling and short molecular dynamics simulations. Considering the recently proposed membrane orientation of a mammalian P450, our CrtS−CrtR model predicts that both N-terminal ends stand adjacent to the membrane plane, allowing their anchoring. Compared with the possible interface between CrtS and both FMNbd, the *Xanthophyllomyces* system appears to be stabilized by more saline bridges.

KEYWORDS: *cytochrome P450 reductase, FMN-binding domain, astaxanthin synthase, protein complex modeling, Xanthophyllomyces dendrorhous*

INTRODUCTION

Carotenoids are naturally occurring pigments with more than 600 different chemical structures described to date. Plants, algae, and some fungi and bacteria produce these pigments; however, animals must get them from their diet, because they are unable to synthesize them de novo.[1] Carotenoids are valued in the food industry as they are widely used as food colorants.[2] Moreover, they have antioxidant properties, which can mitigate the damaging effects of oxidative stress.[3] For this reason, these compounds have also received much attention for their ability to alleviate chronic diseases.[4] A central focus of studies regarding the heterologous production of carotenoids has been the organization of the carotenogenic enzymes that are necessary for the synthesis of the final products in many different organisms.[1]

Xanthophyllomyces dendrorhous is a basidiomycete yeast and is one of the few organisms that produces astaxanthin (3,3′-dihydroxy-β,β-carotene-4,4′-dione), a carotenoid with great commercial potential in the pharmaceutical and food industries.[4] It has been reported that the antioxidant properties of astaxanthin are greater than those of β-carotene or even α-tocopherol.[4] Some of the potential benefits that have been reported for astaxanthin on human health include the prevention of cardiovascular diseases, antibacterial action against *Helicobacter pylori* infections, and stimulation and modulation of the immunological system; also, the supplementation of astaxanthin has been proved to have anticancer activity in mice and rats.[4] On the other hand, astaxanthin has been widely used in the aquaculture industry as a colorant in salmon farming to achieve the color of the flesh that is required by the consumers, having a considerable impact on the production costs,[1] and has also been used to enrich the nutrient value of egg yolks.[2] In addition, the administration of this carotenoid to layer hens improves their health, increases their fertility, and decreases their mortality.[4] In light of the foregoing, the prevalent use of astaxanthin in the food, aquiculture, pharmaceutical, and cosmetic industries, and the increasing demand for natural products, this carotenoid and its natural sources have great commercial potential.

Interestingly, unlike other astaxanthin-producing organisms, in *X. dendrorhous* a single astaxanthin synthase (CrtS) encoded by *crtS* catalyzes the ketolation and hydroxylation of β-carotene to produce astaxanthin.[5,6] Additionally, when *X. dendrorhous* is grown in the presence of aminobenzotriazole, a cytochrome P450 inhibitor, β-carotene accumulates while astaxanthin levels fall, with no significant effect on the total carotenoid levels.[6] This experimental evidence, together with the primary structure analysis of CrtS,[5,6] indicates that CrtS belongs to the cytochrome P450 protein family. Cytochrome P450s are a large superfamily of heme-containing monooxygenases that are present in different organisms from all domains of life. These enzymes play an important role in the oxidative metabolism of a wide range of both exogenous and endogenous substrates according to the general reaction $RH + O_2 + 2e^- + 2H^+ \rightarrow ROH + H_2O$.[7] Two electrons are required for the P450-mediated O_2 activation of the heme iron, which are primarily supplied by NADPH and transferred to the cytochrome P450 enzyme via a redox partner, which, for microsomal cytochrome P450, is generally a cytochrome P450 reductase (CPR).[7] Accordingly, our group has recently demonstrated the

Received: May 25, 2012
Revised: August 13, 2012
Accepted: August 16, 2012
Published: August 16, 2012

involvement of a CPR, encoded by the *crtR* gene, in *X. dendrorhous* astaxanthin biosynthesis.[8]

It has been postulated that the *X. dendrorhous* astaxanthin-producing cytochrome P450 system is unique because CrtS has a high specificity for its own CPR,[9] CrtR. This was proposed because in metabolically engineered *Saccharomyces cerevisiae* strains in which the *X. dendrorhous* carotenogenic genes were introduced, astaxanthin production was only achieved when CrtS was coexpressed with CrtR. However, it should be noted that heterologous expression of several other cytochrome P450s in *S. cerevisiae* has been functionally successful, indicating that the endogenous *S. cerevisiae* CPR (*Sc*CPR, PDB ID 2BF4) is capable of reducing a wide variety of P450s,[7] but not *X. dendrorhous* CrtS. At this point, we highlight the fact that synthesis of astaxanthin from β-carotene through a P450 system has only been reported for *X. dendrorhous*, making this organism not only unique but also very attractive to study.

CPRs are composed of a FMN-binding domain (FMNbd), homologous to bacterial flavodoxin,[10] a ferredoxin-NAD(P)H reductase module, which contains FAD and binds NADPH, and a connecting domain. The FMNbd is attached to the rest of the protein by a flexible hinge region. The first CPRs crystallized revealed a compact structure; however, the deletion of four residues at the hinge region of the *Rattus norvegicus* CPR resulted in different open conformations.[11] These findings suggest that the CPR FMNbd swings between a closed form for internal electron flow and an open conformation for P450 heme reduction.

To the best of our knowledge, the only available crystallographic structure of a cytochrome P450 and a redox partner complex is the one formed between the heme domain and FMNbd of the *Bacillus megaterium* flavocytochrome P450-BM3 (PDB ID 1BVY).[10] The 1BVY complex has been previously used as a template to model hypothetical interfaces between P450 and FMNbds. For example, the interaction between cindoxin reductase, modeled from human CPR (PDB ID 1B1C) and P450cin (PDB ID 1T2B) was deduced by structural superposition over the corresponding domains of P450-BM3, revealing the importance of negatively charged residues in the FMNbd.[12] On the other hand, protein−protein docking methods were used to deduce the interaction surfaces between an *Oryctolagus cuniculus* P450 (PDB ID 1SUO) and one of the open CPR conformations in rat.[11] In this case, the resulting interaction was similar to the one observed in P450-BM3 crystallographic structure.

Taking into account the above information and the advantages of the heterologous production of astaxanthin in an industrial host such as *S. cerevisiae* using the *X. dendrorhous* carotenogenic genes, it is important to understand the specificity of CrtS−CrtR interaction. Thus, the aim of this work was to propose a structure for this complex via protein modeling and optimization through short molecular dynamics simulations (MDS). We address the preference of this association over the possible interaction between CrtS and the FMNbd of *Sc*CPR by comparing features of their modeled protein−protein interfaces. Also, we show that the proposed interaction is in accordance with the open conformations of CPR observed by protein crystallography and the membrane orientation predicted for the human cytochrome P450 2C9.[13] To date, all attempts to produce astaxanthin heterologously using the *X. dendrorhous* carotenogenic genes have been unsuccessful,[6,9] as many aspects of this biosynthetic pathway are still not known. Thus, the information gathered in this work for this particular P450 system may give insights into comprehending the basis for the specificity of CrtS for its own CPR, CrtR.

MATERIALS AND METHODS

Three-Dimensional Protein Modeling. We used the sequences of CrtR (encoding gene GeneBank ID EU884133.1) and CrtS (encoding gene GeneBank ID DQ202402.1) to align against the sequences of their respective structural templates employing ClustalX 2.1.[14] For CrtR, the chosen template was the CPR from *S. cerevisiae*, *Sc*CPR (PDB ID 2BF4), with 38% sequence identity (55% similarity). For CrtS, the chosen templates were structures of human cytochrome P450 3A4 (PDB ID 3NXU) with 29% sequence identity (45% similarity) and cytochrome P450-BM3 from *B. megaterium* (PDB ID 1BVY) with 23% sequence identity (41% similarity).

Three-dimensional model structures of CrtS and CrtR were generated using the program Modeler 9v7.[15] These models did not include the protein membrane spanning regions. Model generation was carried out by the use of the variable target function method employing methods of conjugate gradients and MDS with simulated annealing. Ten models were generated for each protein, and to choose for the best model, their overall quality was assessed using the ProsaII[16] *Z* scores and VERIFY3D.[17] Secondary structure prediction consensus by JPRED 3[18] showed a good correlation (nearly 80%) with the generated models.

Structural superpositions were made with the STAMP tool in VMD 1.9.[19]

Molecular Dynamics Simulations. MDS were performed for the three-dimensional model complex of CrtS−FMNbd from *X. dendrorhous* CrtR (CrtS−*Xd*FMNbd) and for the CrtS−FMNbd from *S. cerevisiae* CPR (CrtS−*Sc*FMNbd) using NAMD 2.8[20] and the CHARMM27[21] force field. The parameters and topology of the FMN molecule were taken from a simulation of the LOV2/LOV1 proteins.[22] The protein was under explicit solvent in a box of TIP3P water molecules with a pad of 15 Å in all directions, and the system charge was neutralized with Na^+ counterions. The simulation was carried out using an integration step of 1 fs, and the nonbonded interactions were considered in a radius of 12 Å with a switching function beyond 10 Å. A conjugate gradient energy minimization of 30000 steps was applied to the system followed by a heating process, raising the temperature gradually to 300 K. During the equilibration process, the force restrictions over the protein backbone were decreased from 5 kcal/mol in 0.1 kcal/mol steps, every 50 ps, until no restrictions were present. Under these conditions, the energy of the system quickly dropped and became completely stable from 6 ns. For the last 4 ns the observed root mean square deviation (rmsd) of the CrtS model (with respect to the initial structure) was 4.9 ± 0.2 Å in the case of its association with *Xd*FMNbd and 5.1 ± 0.3 Å in the case of its association with *Sc*FMNbd. The *Xd*FMNbd model fluctuates considerably less than CrtS (rmsd = 2.0 ± 0.1 Å), but slightly more the crystal structure of *Sc*FMNbd (rmsd = 1.7 ± 0.1 Å).

VMD 1.9 was used to analyze the trajectories by observing the direct salt bridges using a 4 Å distance with a 60° angle cutoff and hydrogen bonds with a 3.2 Å distance and a 60° angle cutoff. Two independent 10 ns trajectories were run for each system (CrtS−*Xd*FMNbd and CrtS−*Sc*FMNbd), resulting in no significant differences for all of the described trends.

Electrostatic Energy Calculation. The PDB2PQR server[23] was used to prepare the structures for continuum electrostatic calculations using the adaptive Poisson−Boltzmann solver. The atom charges and radii were established in accordance with the CHARMM force field, and the protonation states were assigned for the amino acid side chains. The dielectric constants were set to the default values provided by the server (2 for the protein and 78.54 for the solvent).

RESULTS AND DISCUSSION

The availability of 3D protein structures for different P450s and their redox partners is an important step in elucidating the

Table 1. Closest CrtS Homologous Structures Found in PDB[a]

PDB ID	*E* value	coverage (aa)	identities aa (%)	similarity aa (%)	gaps aa (%)	family	organism
3NXU	3.00×10^{-32}	493	144 (29%)	223 (45%)	90 (18%)	3A4	*Homo sapiens*
1BVY	4.00×10^{-22}	424	102 (24%)	178 (41%)	71 (16%)	BM3	*Bacillus megaterium*
3K9V	2.00×10^{-17}	508	116 (22%)	213 (41%)	78 (15%)	24A1	*Rattus norvegicus*
3MDM	1.00×10^{-14}	461	104 (22%)	195 (42%)	75 (16%)	46A1	*Homo sapiens*
3N9Y	5.00×10^{-14}	201	59 (29%)	88 (43%)	28 (13%)	11A1	*Homo sapiens*

[a]BLAST parameters for the top five hits. The query sequence is 557 residues long. aa denotes number of amino acids.

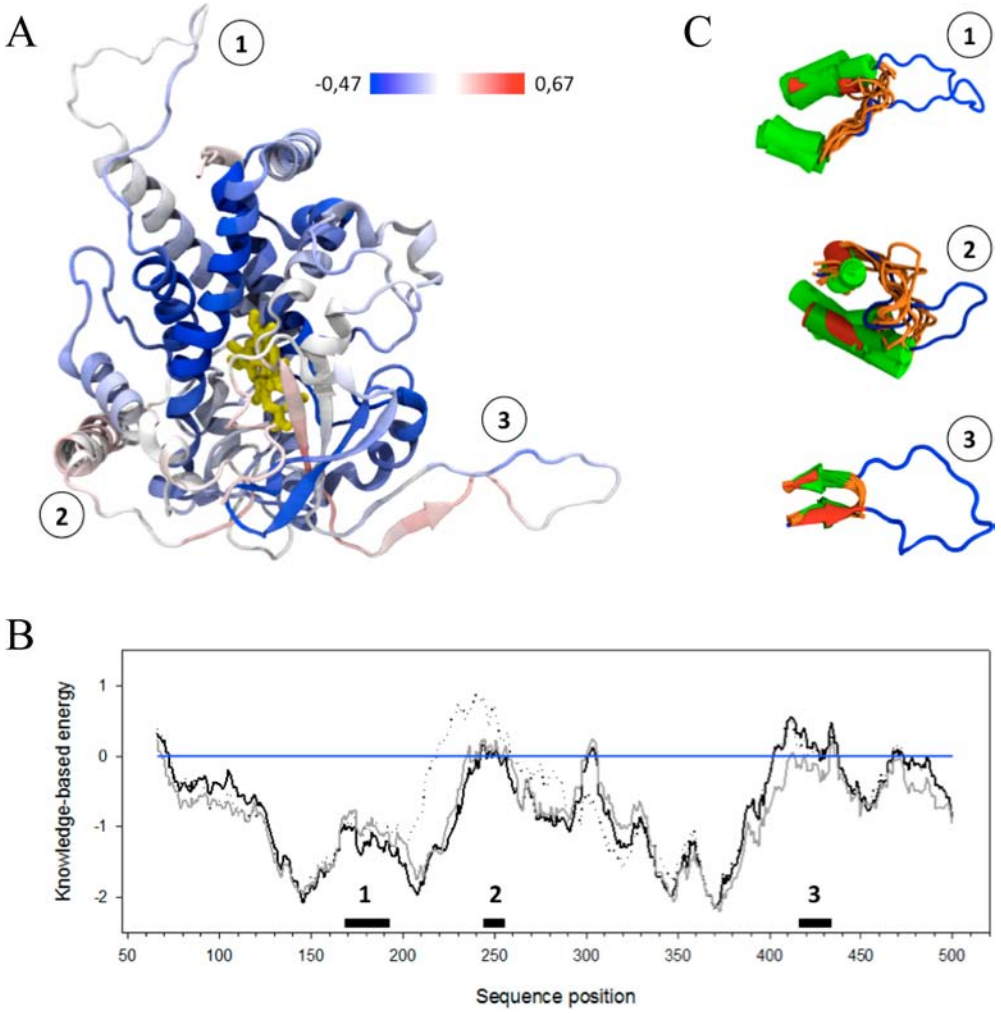

Figure 1. CrtS model, features, and evaluation. (A) Ribbon diagram of CrtS colored according to Verify3D[17] score. The heme group is colored yellow. The numbers designate the three extended loops described in the text. (B) ProsaII[16] energy profile for three stages of the modeling: the initial model (black dashed dots), the model after loop refinement (black solid line), and the model after energy minimization (gray solid line). The 0 score (blue line) indicates the threshold over which poorly evaluated regions are observed. Bold lines indicate the polypeptide sections spanned by the three extended loops. (C) Structural superposition of 24 P450 proteins at the region around the three extended loops. The secondary structures are represented in green (red for CrtS), loops in orange (blue for CrtS).

possible interaction surfaces in specific P450 systems by protein modeling. Initially, we performed a hydropathic profile analysis for CrtS and CrtR and, as expected, it indicated that both have a hydrophobic region at their N-termini (residues 1−35 in CrtS and 1−63 in CrtR) that should allow the P450 system to anchor to the endoplasmic reticulum (ER) membrane.[7] The secondary structure prediction from Jpred[24] strongly suggests the existence of only one helix for both proteins at their predicted transmembrane regions. These hydrophobic regions were excluded from the modeling procedure described below. Both proteins, CrtS and CrtR, were independently modeled using Modeler 9v7.

CrtS Three-Dimensional Structure Modeling. We used the CrtS sequence as input to perform a BLAST[25] search in the entire PDB to find appropriate templates. As shown in Table 1, the top five hits obtained were 3A4, BM3, 24A1, 46A1, and 11A1 cytochrome P450 families. For the resulting alignments, the sequence coverage drops to half of its value after the fourth top hit. Of note is that the second closest hit is the P450−BM3 protein from *B. megaterium* (PDB ID 1BVY), which is the only known X-ray structure describing a complex with an FMNbd.

Table 2. Closest CrtR Homologous Structures Found in PDB[a]

PDB ID	*E* value	coverage (aa)	identities aa (%)	similarity aa (%)	gaps aa (%)	family	organism
2BF4	1.0×10^{-126}	705	272 (38%)	392 (55%)	63 (8%)	P450 reductase	*Saccharomyces cerevisiae*
3QE2	1.0×10^{-109}	697	259 (37%)	373 (53%)	105 (15%)	P450 reductase	*Homo sapiens*
1AMO	1.0×10^{-109}	694	260 (37%)	372 (53%)	98 (14%)	P450 reductase	*Rattus norvegicus*
1TLL	3.00×10^{-44}	742	186 (25%)	324 (43%)	167 (22%)	NO synthase	*Rattus norvegicus*
2QTZ	9.00×10^{-35}	455	118 (25%)	208 (45%)	54 (11%)	MET synthase reductase	*Homo sapiens*

[a]BLAST parameters for the top five hits. The query sequence is 746 residues long. aa, number of amino acids; NO, nitric oxide; MET, methionine.

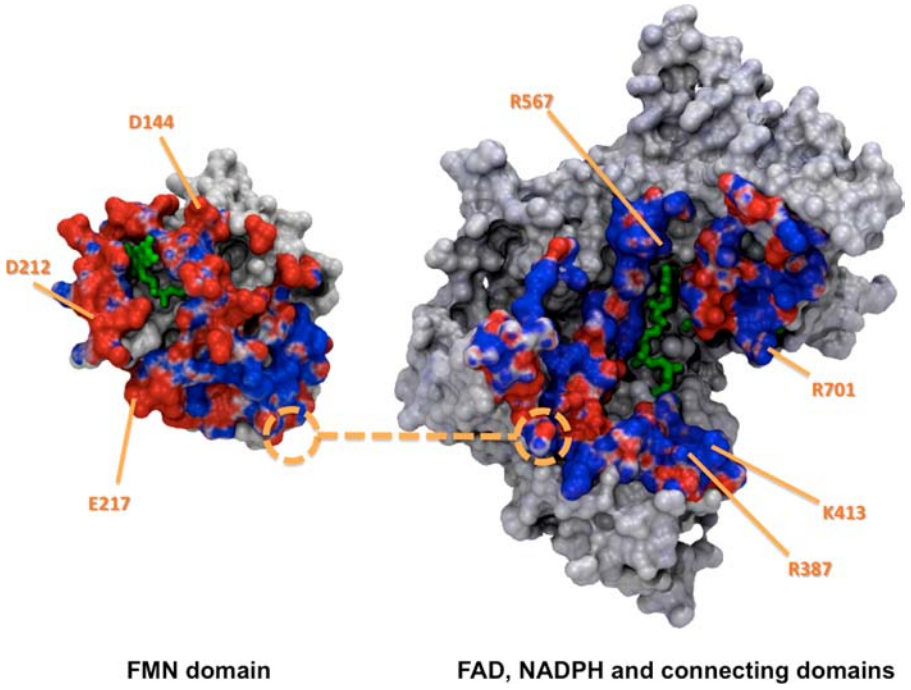

Figure 2. CrtR model and electrostatic surface at the interdomain interface. The Poisson–Boltzmann electrostatic potentials are displayed on the protein surface corresponding to the interface between the FMNbd and the rest of CrtR. The surface coloring ranges from blue for positive charges to red for negative charges, covering ± 5 k_BT/e_c. The FMN and NADPH cofactors are shown in green. Regions outside this interface are colored gray. Orange labels indicate charged residues that are involved in salt bridges. Orange circles indicate where these domains are connected in the polypeptide chain.

Thus, in addition to the closest homologue, the human microsomal P450 3A4 (PDB ID 3NXU), we included 1BVY as a second template for modeling. The resulting structure was further improved by loop refinement and energy minimization protocols. When only 3NXU was used as the template for modeling purposes, several of the CrtS regions had poor evaluation scores that could not be improved by the regular optimization protocols of Modeler (not shown). As depicted in Figure 1, for almost the entire structure the obtained model had good Verify3D[17] (Figure 1A) and ProsaII[16] (Figure 1B) scores. In the final CrtS three-dimensional model, most of the best-evaluated residues (blue regions) lie in the neighborhood of the heme cofactor (in yellow, Figure 1A).

The final model has three extensive loops comprising residues 169–192, 244–255, and 417–432 (indicated by consecutive numbers in Figure 1). Indeed, the Jpred predictor[24] does not favor secondary structure formation within these regions. Moreover, all known P450 structures (including the templates) have shorter loops in the equivalent regions (Figure 1C). When considering the interaction with CrtR and membrane orientation (see below), we suggest that these loops may have a role in protein complex formation and interaction with the ER membrane.

CrtR Three-Dimensional Structure Modeling. In the case of CrtR modeling, a BLAST search of the PDB retrieved the CPR from *S. cerevisiae*, *Sc*CPR (PDB ID 2BF4) at the top of the hit list, with 38% sequence identity (55% similarity) and the lowest percentage of gaps (Table 2). Only three nonredundant P450 reductases are deposited in the PDB, one from *S. cerevisiae* and two from mammals. Taken together, Tables 1 and 2 show that sequence conservation is higher among CPRs (37% identity with the *H. sapiens* and *R. norvegicus* CrtR homologues) than in P450 enzymes (22–29% identity with the *H. sapiens* and *R. norvegicus* CrtS homologues). The sole use of *Sc*CPR as the template to model CrtR resulted in good scores (Verify3D[17] and ProsaII[16]) in all of the multidomain structures (not shown). The structure of 2BF4 (as well as the other wild type CPRs that have been crystallized) represents the closed conformation[26] of *Sc*CPR that allows electron transfer from NADPH to FAD to FMN, but is incompatible for the electron transfer from FMN to the heme in the cytochrome P450 protein. Several lines of evidence[11,27,28] indicate that, to shuttle electrons to the P450 redox partner, this protein must suffer a conformational change, exposing the FMN cofactor and breaking the interactions with the rest of the reductase domains. Thus, several residues participating in interfacial

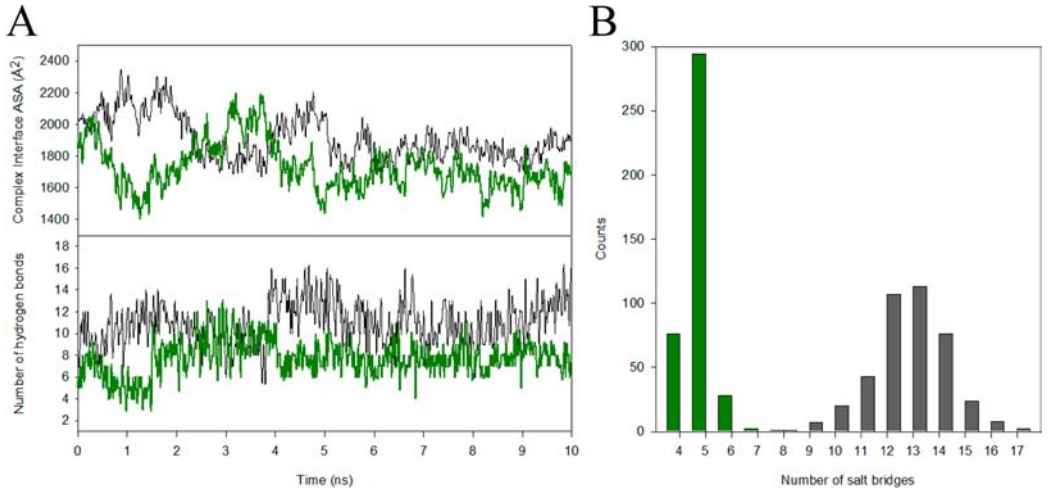

Figure 3. Molecular dynamics simulation of alternative CrtS−FMNbd complexes: (A) time course of the interfacial surface area (ASA; upper panel) and the average number of hydrogen bonds (lower panel) between CrtS and either *Xd*FMNbd (dark line) or *Sc*FMNbd (green line); (B) distribution of the number of saline bridges formed between the alternative complexes during the last 4 ns of the simulation. Bar colors according to panel A.

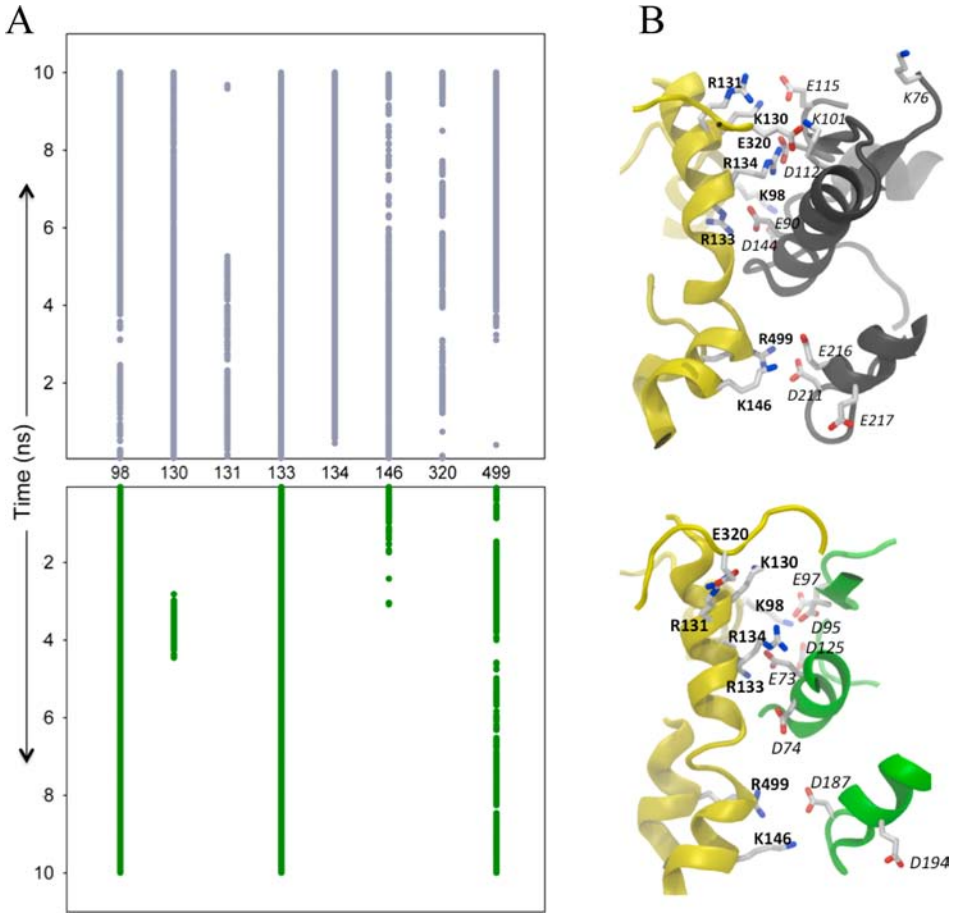

Figure 4. Salt bridge patterns in alternative CrtS−FMNbd interfaces. (A) The CrtS residues that are involved in salt bridges with either *Xd*FMNbd (upper panel) or *Sc*FMNbd (lower panel) are shown on the *x*-axis. The *y*-axis indicates whether these residues form a salt bridge with residues from the corresponding FMNbd during the trajectory. (B) Ribbon diagrams of the two alternative complex structures around the interfacial region, at the end of the 10 ns simulation. CrtS is colored yellow, *Xd*FMNbd, gray, and *Sc*FMNbd, green. The specific residues forming salt bridges are labeled in **bold** for CrtS and in *italics* for FMNbd and colored according to the CPK code (white for carbon, blue for nitrogen, and red for oxygen).

contacts with the P450 protein are also involved in the interdomain interface of closed CPR.[28] Figure 2 shows the electrostatic features of the interdomain interaction surface of CrtR. Even though there is a clear electrostatic complementarity, only three acidic residues (D144, D212, and E217) in the FMNbd are involved in forming direct saline bridges with four

dx.doi.org/10.1021/jf302287f | J. Agric. Food Chem. 2012, 60, 8640−8647

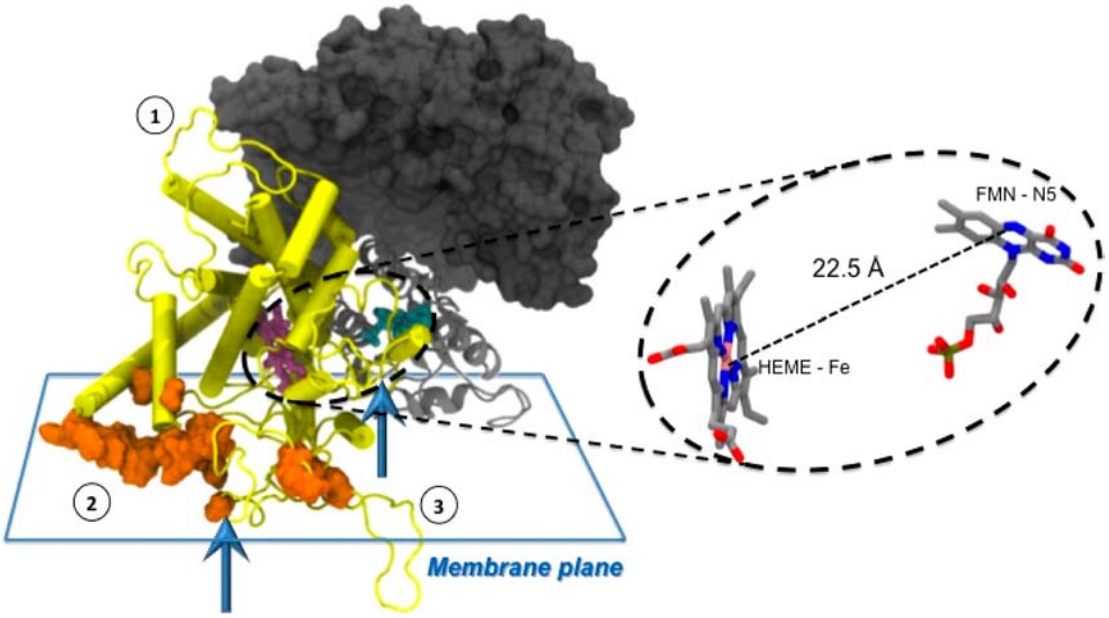

Figure 5. Scheme of the CrtS−CrtR complex positioned in the membrane. The CrtS model is colored yellow. Orange surfaces denote residues aligning to those in human cytochrome P450 2C9, simulated by Cojocaru[13] and known to be in contact with the membrane. For CrtR, FMNbd is shown as gray ribbons, and the rest of the protein, shown as a gray surface, was taken from the open conformation of rat CPR (PDB ID 3ES9, chain A) upon superposition of the corresponding FMNbds. The heme and FMN molecules are colored in mauve and cyan, respectively. An imaginary plane representing the membrane surface is sketched to illustrate the regions potentially in contact with the membrane and the location of the N-terminal end of each structure (blue arrows). The distance between the N5 atom in the FMN molecule and the Fe atom in the heme molecule, at the end of the simulation, is also shown.

basic residues (R387, K413, R567, and R701) in the other domains of the reductase. Upon complex formation, two of these negative residues become engaged in saline bridges with CrtS (see below). In our model, the loop or *hinge* that connects the FMNbd with the other domains of CrtR is 11 residues long, which is within the reported minimum length required for electron transfer to its physiological redox partner.[11]

Interfacial Interactions between CrtS and Alternative FMN-Binding Domains. To date, the structures of 40 nonredundant P450 proteins are deposited in the PDB, 23 from eukaryotic organisms, 15 from bacteria, and 2 from archaea. Among them, the 1BVY structure stands as an archetype of the oligomeric arrangement between P450s and the FMNbd of CPRs. For example, Sirim and co-workers[29] used this structure as a superposition pattern to perform a systematic comparison of the interaction surface between several cytochrome P450s and the FMNbd of the *R. norvegicus* CPR. Because CrtS recovers 1BVY as one of the closest structural homologues (Table 1, top blast hits), it is reasonable to expect that the packing seen in the *B. megaterium* complex would be conserved in the *Xanthophyllomyces* system. To gain insights about the possible reason why CrtS is not functional in *S. cerevisiae* unless it is coexpressed with CrtR, we modeled the interaction of CrtS with its two possible redox partners, the FMNbd of CrtR and *Sc*CPR (*Xd*FMNbd and *Sc*FMNbd, respectively). The relative position of the heterocomplex members was taken from the heme-binding domain and the flavodoxin domain in the crystal structure of *B. megaterium* P450-BM3 (PDB ID 1BVY). The CrtS model was superposed over the heme-binding domain of P450-BM3 and either *Xd*FMNbd (residues 64−236) or *Sc*FMNbd (residues 59−213) over the flavodoxin domain. The initial structure for both complexes was relaxed through energy minimization in the presence of water molecules. The resulting interfacial area was 2139 Å^2 for the CrtS complex with CrtR and 1972 Å^2 for the complex with *Sc*CPR. Thus, the built heterodimers served as the starting point for MDS using NAMD. The trajectories were evaluated for three key indicators of interaction stability: changes in the interfacial surface area, mean number of hydrogen bonds, and mean number of salt bridges (Figure 3).

The surface area of the interaction is marginally greater in the CrtS−*Xd*FMNbd complex than in CrtS−*Sc*FMNbd. For example, during the 9th ns, this area was 1.1-fold greater than in the complex with *Sc*FMNbd. Also, for 69% of the trajectory time, the interfacial area of the interaction between CrtS and *Xd*FMNbd was at least 100 Å^2 higher than the corresponding value in the CrtS−*Sc*FMNbd complex (Figure 3A, upper panel). With regard to the number of hydrogen bonds between the members of the complex (Figure 3A, lower panel), a higher number was observed for the cognate pair: approximately 12 versus 8 in the complex with *Sc*FMNbd, during the final nanosecond (Figure 3A, lower panel). Finally, although the measured distance between the center of mass of the heme and FMN coenzymes was similar in both complexes, the CrtS−CrtR pair showed lower values than CrtS−*Sc*FMNbd, reaching 22.5 Å in contrast to 24.5 Å, respectively, at the end of the 10 ns simulation (data not shown). This value was even slightly shorter than observed for the P450-BM3 X-ray structure (23.6 Å).

Nevertheless, a substantial difference between the tested model complexes appeared when the mean numbers of salt bridges were compared. We quantified the number of saline bridges during the final 4 ns and observed their cumulative distribution for each complex. In the case of CrtS−*Xd*FMNbd, the most frequent value was 13 saline bridges (Figure 3B) compared to 5 in the case of CrtS−*Sc*FMNbd. Not only is the mean number different between the two complexes modeled, but also the pattern of the residues involved in saline bridges

dx.doi.org/10.1021/jf302287f | J. Agric. Food Chem. 2012, 60, 8640−8647

differs. Figure 4 shows the time course of the saline bridge contacts formed by residues of CrtS with each partner. It can be appreciated that residues K98, R133, and R499 could satisfy interactions with both FMNbds. However, residues K130, R134, K146, and E320 formed stable saline bridges only with the *X. dendrorhous* complex. In the case of the interaction with the *Sc*FMNbd, residues K130 and K146 seem to contribute marginally to the intersubunit interaction. For residue R131, a longer simulation would be required to establish its contribution to the interaction of CrtS with the CrtR FMNbd. Our modeling indicates that, on average, 8 more saline bridges are formed between CrtS and associated *Xd*FMNbd than with *Sc*FMNbd (Figure 3). Compared with the possible interface between CrtS and *Sc*FMNbd, the *Xanthophyllomyces* system appears to be stabilized by a higher number of saline bridges. Although several other reasons could explain why there is no production of astaxanthin in *Saccharomyces* upon heterologous expression of CrtS, if a complex between the *Sc*FMNbd and CrtS is formed, our results suggest that it would be not as stable as in CrtS−*Xd*FMNbd for electron transference from FMN to heme.

The importance of saline bridges at the CPR−P450 interface has been addressed previously. Hamdane and colleagues[11] studied the interaction between cytochrome P450 2B4 (PDB ID 1SUO) and one of the CPR "open" conformations found by crystallography through protein−protein docking methods. They identified six basic residues in cytochrome P450 2B4, which were also previously found by site-directed mutagenesis studies,[30] involved in forming electrostatic interactions with its partner protein. Structural alignment of cytochrome P450 2B4 and our CrtS model shows that the overall distribution of the residues involved in the protein−protein interaction was similar in the reported protein docking approximation and our simulation (not shown).

CrtS−CrtR Complex and Membrane Insertion. Another biologically relevant feature is the compatibility between our proposed CrtS−*Xd*FMNbd interface and the insertion of the whole complex on the ER membrane. Cojocaru and colleagues[13] described a protocol that combines coarse-grained and all-atom molecular simulations of the membrane-bound human cytochrome P450 2C9 to understand how the membrane influences its structure, dynamics, and ability to bind substrates. Two different orientations relative to the membrane plane (denominated 1R9OH1 and 1R9OH2) were the most energetically favored. These authors anticipate that one of them, 1R9OH2, might be more efficient for electron transfer between CPR and cytochrome P450. For this reason, they suggest investigating the complex by including CPR in the simulation protocol. In this context, our present report provides the antecedent that using 1BVY as a template for packing cytochrome P450 and CPR is consistent with the putative orientation of the N-terminal transmembrane helix of both redox partners. To illustrate our point, using our model of the interaction between CrtS and FMNbd of CrtR at the end of the 10 ns simulation, we mapped on CrtS the residues homologous to those predicted to be in contact with the membrane in the 1R9OH2 configuration of cytochrome P450 2C9[13] (Figure 5). When these residues are located relative to a plane (representing the ER membrane), the N-terminal ends of both proteins, CrtS and CrtR, align very close to that plane. Conversely, when repeating this exercise with 1R9OH1, we observe a different arrangement, inconsistent with membrane insertion (not shown). It is interesting to note that extended loops 2 and 3, composed of residues A244−T255 and P417−E432, respectively (Figure 1A), appear to be embedded within the lipid bilayer. This observation suggests that, in addition to the predicted N-terminal transmembrane helix, two other regions of the polypeptide could be playing an important role in anchoring CrtS to the membrane. Furthermore, the relative location of extended loop 1 in CrtS, including residues E169−D192, lies very close to the FAD domain of CrtR (Figure 5). Thus, in addition to the presently reported protein−protein interface, other possible interfaces can be implied when the whole CrtR protein is taken into account. In a future approach and to obtain a precise picture of the functions of the extended loops, it will be highly informative to simulate the entire CrtS and CrtR complex, considering both the complete CrtR structure and the membrane environment.

The structural characteristics of the interface between P450 and CPR determine the rate of electron transfer. Although the importance of electrostatic interactions has been previously addressed, a molecular simulation approach to analyze the interfacial properties of P450 CPR complexes has not been implemented before (to the best of our knowledge). Our results indicate that the electrostatic interactions, and specifically the number of saline bridges, are the feature that better explains the preference of CrtS for *Xd*FMNbd. Finally, this work could help to advance the rational design of the P450−CPR interaction, to optimize the expression of P450 systems in heterologous hosts such as *Saccharomyces*. This yeast has powerful advantages for growth and molecular biology manipulations, and it is the most convenient platform for pigment production.

AUTHOR INFORMATION

Corresponding Author

*Phone: 56-2-9787316. Fax: 56-2-2727363. E-mail: vcifuentes@uchile.cl.

Funding

This work was supported by Universidad de Chile VID Iniciación I 10/01-2 for J.A., Fondecyt 1100324 for V.C., and Fondecyt 1121170 for R.C.

Notes

The authors declare no competing financial interest.

ACKNOWLEDGMENTS

We thank Michael Handford for proofreading the manuscript and Gabriela Contreras for the *X. dendrorhous* strain picture used in the TOC graphic.

ABBREVIATIONS USED

CPR, cytochrome P450 reductase; ER, endoplasmic reticulum; FAD, flavin adenine dinucleotide; FMN, flavin mononucleotide; FMNbd, FMN binding domain; MDS, molecular dynamics simulations; NADPH, nicotinamide adenine dinucleotide phosphate; P450, cytochrome P450; PDB, Protein Data Bank; ScCPR, *S. cerevisiae* cytochrome P450 reductase; ScFMNbd, *S. cerevisiae* FMN binding domain; XdFMNbd, *X. dendrorhous* FMN binding domain

REFERENCES

(1) Britton, G.; Liaaen-Jensen, S.; Pfander, H. *Carotenoids. Vol. 3: Biosynthesis and Metabolism*; Birkhäuser: Basel, Switzerland, 1998.

(2) Walker, L. A.; Wang, T.; Xin, H.; Dolde, D. Supplementation of laying-hen feed with palm tocos and algae astaxanthin for egg yolk nutrient enrichment. *J. Agric. Food Chem.* **2012**, *60*, 1989−1999.
(3) Kim, Y. J.; Kim, Y. A.; Yokozawa, T. Protection against oxidative stress, inflammation, and apoptosis of high-glucose-exposed proximal tubular epithelial cells by astaxanthin. *J. Agric. Food Chem.* **2009**, *57*, 8793−8797.
(4) Higuera-Ciapara, I.; Felix-Valenzuela, L.; Goycoolea, F. M. Astaxanthin: a review of its chemistry and applications. *Crit. Rev. Food Sci. Nutr.* **2006**, *46*, 185−196.
(5) Álvarez, V.; Rodríguez-Sáiz, M.; de la Fuente, J. L.; Gudiña, E. J.; Godio, R. P.; Martín, J. F.; Barredo, J. L. The *crtS* gene of *Xanthophyllomyces dendrorhous* encodes a novel cytochrome-P450 hydroxylase involved in the conversion of β-carotene into astaxanthin and other xanthophylls. *Fungal Genet. Biol.* **2006**, *43*, 261−272.
(6) Ojima, K.; Breitenbach, J.; Visser, H.; Setoguchi, Y.; Tabata, K.; Hoshino, T.; van den Berg, J.; Sandmann, G. Cloning of the astaxanthin synthase gene from *Xanthophyllomyces dendrorhous* (*Phaffia rhodozyma*) and its assignment as a β-carotene 3-hydroxylase/4-ketolase. *Mol. Genet. Genomics* **2006**, *275*, 148−158.
(7) van den Brink, H.; van Gorcom, R. F. M.; van den Hondel, C. A.; Punt, P. J. Cytochrome P450 enzyme systems in fungi. *Fungal Genet. Biol.* **1998**, *23*, 1−17.
(8) Alcaíno, J.; Barahona, S.; Carmona, M.; Lozano, C.; Marcoleta, A.; Niklitschek, M.; Sepúlveda, D.; Baeza, M.; Cifuentes, V. Cloning of the cytochrome p450 reductase (*crtR*) gene and its involvement in the astaxanthin biosynthesis of *Xanthophyllomyces dendrorhous*. *BMC Microbiol.* **2008**, *8*, 169.
(9) Ukibe, K.; Hashida, K.; Yoshida, N.; Takagi, H. Metabolic engineering of *Saccharomyces cerevisiae* for astaxanthin production and oxidative stress tolerance. *Appl. Environ. Microbiol.* **2009**, *75*, 7205−7211.
(10) Sevrioukova, I. F.; Li, H.; Zhang, H.; Peterson, J. A.; Poulos, T. L. Structure of a cytochrome P450−redox partner electron-transfer complex. *Proc. Natl. Acad. Sci. U.S.A.* **1999**, *96*, 1863.
(11) Hamdane, D.; Xia, C.; Im, S. C.; Zhang, H.; Kim, J. J.; Waskell, L. Structure and function of an NADPH-cytochrome P450 oxidoreductase in an open conformation capable of reducing cytochrome P450. *J. Biol. Chem.* **2009**, *284*, 11374−11384.
(12) Kimmich, N.; Das, A.; Sevrioukova, I.; Meharenna, Y.; Sligar, S. G.; Poulos, T. L. Electron transfer between cytochrome P450cin and its FMN-containing redox partner, cindoxin. *J. Biol. Chem.* **2007**, *282*, 27006−27011.
(13) Cojocaru, V.; Balali-Mood, K.; Sansom, M. S. P.; Wade, R. C. Structure and dynamics of the membrane-bound cytochrome P450 2C9. *PLoS Comput. Biol.* **2011**, *7*, e1002152.
(14) Larkin, M. A.; Blackshields, G.; Brown, N. P.; Chenna, R.; McGettigan, P. A.; McWilliam, H.; Valentin, F.; Wallace, I. M.; Wilm, A.; Lopez, R. Clustal W and Clustal X version 2.0. *Bioinformatics* **2007**, *23*, 2947−2948.
(15) Sali, A.; Blundell, T. L. Comparative protein modelling by satisfaction of spatial restraints. *J. Mol. Biol.* **1993**, *234*, 779−815.
(16) Sippl, M. J. Recognition of errors in three-dimensional structures of proteins. *Proteins* **1993**, *17*, 355−362.
(17) Eisenberg, D.; Lüthy, R.; Bowie, J. U. VERIFY3D: Assessment of protein models with three-dimensional profiles. *Methods Enzymol.* **1997**, *277*, 396−404.
(18) Jones, D. T. Protein secondary structure prediction based on position-specific scoring matrices 1. *J. Mol. Biol.* **1999**, *292*, 195−202.
(19) Humphrey, W.; Dalke, A.; Schulten, K. VMD: visual molecular dynamics. *J. Mol. Graph.* **1996**, *14*, 33−38.
(20) Phillips, J. C.; Braun, R.; Wang, W.; Gumbart, J.; Tajkhorshid, E.; Villa, E.; Chipot, C.; Skeel, R. D.; Kale, L.; Schulten, K. Scalable molecular dynamics with NAMD. *J. Comput. Chem.* **2005**, *26*, 1781−1802.
(21) MacKerell, A. D.; Bashford, D.; Bellott, M.; Dunbrack, R. L.; Evanseck, J. D.; Field, M. J.; Fischer, S.; Gao, J.; Guo, H.; Ha, S.; Joseph-McCarthy, D.; Kuchnir, L.; Kuczera, K.; Lau, F. T. K.; Mattos, C.; Michnick, S.; Ngo, T.; Nguyen, D. T.; Prodhom, B.; Reiher, W. E.; Roux, B.; Schlenkrich, M.; Smith, J. C.; Stote, R.; Straub, J.; Watanabe, M.; Wiorkiewicz-Kuczera, J.; Yin, D.; Karplus, M. All-atom empirical potential for molecular modeling and dynamics studies of proteins. *J. Phys. Chem. B* **1998**, *102*, 3586−3616.
(22) Freddolino, P. L.; Dittrich, M.; Schulten, K. Dynamic switching mechanisms in LOV1 and LOV2 domains of plant phototropins. *Biophys. J.* **2006**, *91*, 3630−3639.
(23) Dolinsky, T. J.; Nielsen, J. E.; McCammon, J. A.; Baker, N. A. PDB2PQR: an automated pipeline for the setup of Poisson−Boltzmann electrostatics calculations. *Nucleic Acids Res.* **2004**, *32*, W665−W667.
(24) Cole, C.; Barber, J. D.; Barton, G. J. The Jpred 3 secondary structure prediction server. *Nucleic Acids Res.* **2008**, *36*, W197−W201.
(25) Altschul, S. F.; Gish, W.; Miller, W.; Myers, E. W.; Lipman, D. J. Basic local alignment search tool. *J. Mol. Biol.* **1990**, *215*, 403−410.
(26) Lamb, D. C.; Kim, Y.; Yermalitskaya, L. V.; Yermalitsky, V. N.; Lepesheva, G. I.; Kelly, S. L.; Waterman, M. R.; Podust, L. M. A second FMN binding site in yeast NADPH-cytochrome P450 reductase suggests a mechanism of electron transfer by diflavin reductases. *Structure* **2006**, *14*, 51−61.
(27) Ellis, J.; Gutierrez, A.; Barsukov, I. L.; Huang, W. C.; Grossmann, J. G.; Roberts, G. C. K. Domain motion in cytochrome P450 Reductase. *J. Biol. Chem.* **2009**, *284*, 36628.
(28) Laursen, T.; Jensen, K.; Møller, B. L. Conformational changes of the NADPH-dependent cytochrome P450 reductase in the course of electron transfer to cytochromes P450. *Biochim. Biophys. Acta−Proteins Proteomics* **2011**, *1814*, 132−138.
(29) Sirim, D.; Widmann, M.; Wagner, F.; Pleiss, J. Prediction and analysis of the modular structure of cytochrome P450 monooxygenases. *BMC Struct. Biol.* **2010**, *10*, 34.
(30) Bridges, A.; Gruenke, L.; Chang, Y. T.; Vakser, I. A.; Loew, G.; Waskell, L. Identification of the binding site on cytochrome P450 2B4 for cytochrome b5 and cytochrome P450 reductase. *J. Biol. Chem.* **1998**, *273*, 17036−17049.